

Direct Imaging of Two-Phase Flows by Electrical Impedance Measurements

Eric HERVIEU* and Paulo SELEGHIM Junior[#]

*Commissariat à l'Energie Atomique, DRN / DTP / SMTH / LATA
38054 Grenoble cedex 9, France
eric.hervieu@cea.fr

[#]Universidade de São Paulo, EESC – SEM, Av. Dr. Carlos Botelho, 1465
13560-970 São Carlos – SP, Brazil
seleghim@sc.usp.br

Abstract - This paper presents a two-phase flow direct imaging sensor, based on multiple electrical impedance measurements. The electrode configuration is optimized to provide imaged information on the phase distribution within the probe's sensing volume. As a consequence, the time evolution of the flow topology can be represented by simply plotting the signals corresponding to the peripheral impedance measurements, and therefore needs no numerical reconstruction from the experimental data. Several transient tests are performed in a two-phase air-water loop. They demonstrate that the sensor exhibits not only large structures such as slugs and plugs, but also some finer details such as the wavy or rugged interface in stratified flow, or such as the liquid film drainage during the transition between intermittent and annular flows. The methodology proposed in the present work constitutes a simple and inexpensive alternative to tomographic imaging techniques, and is thus fully adapted to online process monitoring of multiphase flow systems.

Keywords : Flow Monitoring – Impedance Sensor – Direct Imaging – Two-Phase Flows.

1. INTRODUCTION

Process imaging techniques allow to investigate inside complex structures such as the phase geometrical organization of gas-liquid mixtures. They provide detailed information about the phenomenology governing multiphase flows and are helpful to understand their fundamental hydrodynamics. As a consequence, such techniques are of great interest to improve the design and operation of multiphase flow equipment and systems. The need for visualization techniques is well identified, as revealed by the rapidly increasing number of scientific publications on this subject. Furthermore, investigation must frequently involve non-invasive instruments, to avoid process disturbance and because of severe experimental conditions.

This paper describes a direct two-phase flow qualitative imaging technique based on electrical impedance measurements. More specifically, in order to obtain an imaged representation of the flow pattern from peripheral measurements, one has generally to solve an inverse problem, which is intrinsically ill-posed in a numerical point of view (Lemonnier & Peytraud [1]). In what concerns electrical techniques, the main critical

drawback of this ill-posedness is the non-uniqueness of the reconstructed solution with respect to any set of measurements (Seo [2]). Our approach is to avoid the numerical image reconstruction procedure by adapting the geometry of the sensing device in a way that the main features of the flow pattern become evident by simply plotting the probe's unprocessed signals. This procedure is justified by the fact that, in many multiphase systems monitoring tasks, one needs only to have an approximate and qualitative representation of the phase spatial distribution in the flowing mixture. Consequently, the direct imaging approach is a simple and inexpensive alternative to tomographic imaging techniques.

2. TOMOGRAPHIC IMAGING

In order to obtain a phase profile corresponding to the multiphase flow pattern, the most common approach is to install several sensors around the pipe or vessel confining the flow. This is done in such a way that the output signal of each sensor depends on the constitution of the fluid within its sensing zone. In other words, most imaging techniques exploit differences or contrasts in some physical properties between the phases of the multiphase mixture.

Subsequently, a computer may be used to reconstruct from these signals a 2D or a 3D image of the flow, using a tomographic inversion technique. Depending on the physical principle of the sensing system, the measured signals may contain information related to a well-delimited region inside the sensing volume. Examples of this are transmission/emission methods like nucleonic techniques (X-ray, γ -ray attenuation or single photon and positron emission) as well as some acoustic and optical methods. There are several reconstruction algorithms suited for this type of problem such as, for instance, Fourier inversion, convolutional back-projection and algebraic reconstruction methods (Herman [3]; Natterer [4]).

In opposition with transmission/emission methods, the peripheral signals obtained from diffraction (neutron, γ -ray and acoustic wave scattering) or electrical sensing systems result from undetermined regions within the sensing zone. How much each of these regions contributes to the measured values depends on the unknown phase distribution of the multiphase fluid. This feature, referred to as the soft-field effect, requires refined numerical reconstruction techniques. Problems issued from diffractive or scattering systems can be usually solved by means of algorithms based on moment and pseudo inversion methods (Caorsi *et al.* [5]; Chiu *et al.* [6]). Problems issued from electric sensing systems can be frequently treated with several back-projection methods (Huang *et al.* [7]; Xie *et al.* [8]) and by means of iteration algorithms based on optimization techniques (Isaksen & Nordtvedt [9]), perturbation methods (Kim & Woo [10]; Yorkey *et al.* [11]) or the Newton-Raphson method (Yorkey *et al.* [12]; Abdullah *et al.* [13]).

In general, reconstructing an image from peripheral signals by a tomographic technique requires to solve an inverse problem. More specifically, the measurements performed at the periphery provide a set of projected views of the process under investigation, which are then used to construct a cross section profile of the flow pattern. Inverse problems are characteristic of a very large number of mathematically ill-posed problems emerging in physical as well as in medical sciences and others. This ill-posed nature of the problem may, under certain circumstances, affect the quality of the final images. In what concerns multiphase flow tomographic imaging, experimental uncertainties and noise, coupled with round-off and truncation errors inherent to the numerical reconstruction algorithms, may be amplified and corrupt the precision of the results. For instance, when considering the spatial resolution attainable by different sensing methods, it is known that transmission/emission techniques are in general capable of locating an object within 1% of the

sensing zone cross section diameter, while typical resolutions associated to acoustical and electrical techniques correspond to 3% and 10% respectively (Williams & Beck [14]). Another important feature is the "distinguishability" as defined by Gisser *et al.* [15], that is the ability to distinguish between two different phase profiles. Unfortunately, a systematic study dedicated to this subject has not been published yet.

Imaging systems based on electrical measurement are, among other advantages, simple, robust and fast. This explains the great interest presently devoted to process imaging, in the particular field of multiphase flow visualization. However, this technique has some drawbacks. In opposition to X-ray and other transmission/emission techniques, the electrical field is "soft" in the sense that it depends on the phase distribution within the sensing zone. Thus, the forward and the inverse problems are coupled, quantitative reconstruction algorithms are in general iterative and convergence may become a major source of problems. In addition, the algorithms available for image reconstruction assume in general the electrical field to be static and two-dimensional. Calculation results may consequently exhibit some over and under-shooting as for instance void fractions above 100% and under 0% (Xie *et al.* [8]). In the same way, 3D effects lead to the presence of "phantom objects" in the reconstructed images, when the flow configuration is not bidimensional (Peytraud [16]).

These problems motivated us to develop a direct imaging sensor, providing qualitative information on the phase distribution of a flowing multiphase mixture. In order to avoid any numerical reconstruction procedure, the imaging technique is based on visualization of the measured signals. The advantages of such a system are evident, especially in the industrial context where robust and reliable monitoring devices are required for the real-time control of multiphase equipment.

3. DIRECT IMAGING

In order to obtain an image of the flow directly from the measured physical quantities, i.e. without reconstructing it by solving an inverse problem, the sensing technique must divide the sensing region in a certain number of independent sub-regions. If this can be done, each of the measured signals ideally reflects the constitution of the flow within its associated sub-region, independently of the surrounding ones. For example, an ideal imaged representation of the void fraction profile could be obtained by partitioning the investigated volume with multiple phase detectors, the sensing region of each one being restricted to a small region around itself. The set of signals obtained in this way could be directly plotted with respect to the structure of the

partition and, as each value is representative of the local void fraction, the result would be close to the real phase profile, as illustrated in Figure 1. In spite of its ability to produce an ideal image, this measurement procedure would be highly intrusive and difficult to implement in a practical way.

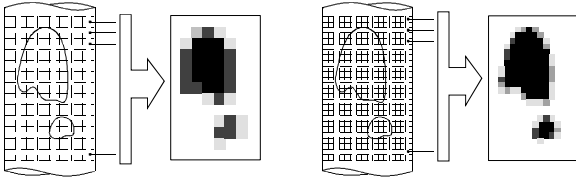


Figure 1: Ideal direct imaging of the phase profile by a set of intrusive local void sensors.

Producing a partition of the investigated volume by means of non-intrusive sensing techniques is a very complex problem and, in our knowledge, no specific work on this subject has been published yet. In the context of electrical measurement techniques, obtaining a regular and constant partition is probably impossible, since it is impossible to precisely confine the electrical field and to know *a priori* its shape. However, a particular excitation / measurement electrode configuration may induce an electrical field sectorized in a way that a measurement variation on a specific electrode could be related to the presence of obstacles within its corresponding sensing sector. This is effectively what has been done in this work, as described in the following.

In the scope of using the imaging technique proposed here in some practical applications such as two-phase flow regime monitoring, two basic requirements were taken into account when defining the configuration of the electrodes:

- the probe should not disturb the flow (what excludes the use of wires)
- the probe should have a limited measuring volume in order to reduce the longitudinal averaging effect and to increase the resolution in this direction (what restricts the adoption of long longitudinal measuring electrodes such as for instance proposed by Klug & Mayinger [17] and

Huang *et al.* [7]).

Considering these requirements, the geometry that seemed the most appropriate consists of two stainless steel ring electrodes flush mounted inside the tube, as illustrated in Figure 2. This configuration has been already adopted by Asali *et al.* [18] to measure thin liquid films and by Andreussi *et al.* [19] to measure the liquid hold-up in gas-liquid pipe flows. As already mentioned, the measurement method is based on the difference in the electrical properties of the constitutive phases of the flowing mixture. As a consequence of this contrast, the spatial phase distribution affects the global impedance between the ring electrodes. The probe's working principle corresponds to impose an electrical potential difference between the electrodes and to measure the resulting current at each electrode. More specifically, in two phase flows where only one of the phases is conductive, the impedance may be reduced to a purely resistive contribution when the excitation signal is of sufficiently high frequency so that the contact impedance resulting from electrochemical phenomena taking place near the electrodes becomes negligible (above 1 kHz for conductance's around $0.3 \text{ m}\Omega^{-1}$, *i.e.* tap water). In addition, the excitation frequency must not be excessively high (less than 1 MHz in our case) in order to avoid unwanted electromagnetic effects. Taking into account the quantitative results of impedance analysis measurements and some other requirements concerning the electronics, we chose an excitation frequency of 20 kHz. It is interesting to note that for non-conducting fluids, the direct imaging technique proposed in this work can still be implemented if based on capacitance measurement.

A fundamental characteristic of the ring electrode geometry is that the global impedance is strongly coupled with the flow pattern within the sensing volume, as reported by both Asali *et al.* [18] and Andreussi *et al.* [19]. This can be attributed to strong differences in the current flux distribution in the azimuthal direction with respect to distinct flow regimes. Consequently, a partition

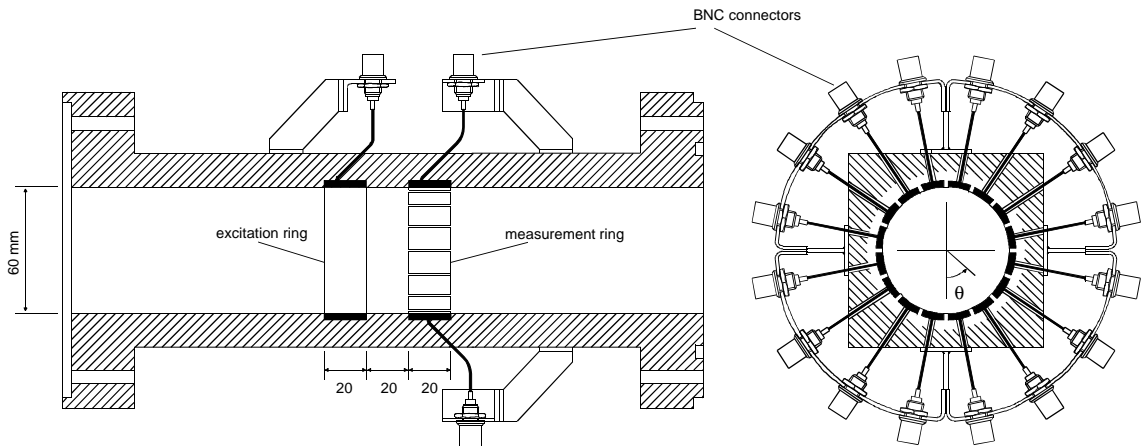


Figure 2: Side and front section views of the conductivity probe (drawn in scale). The symbol θ defines the angular position of the electrodes ($\theta = 0$ or 2π is the bottom and $\theta = \pm \pi$ corresponds to the top of the tube).

of the sensing volume can be obtained by segmenting the measurement ring, what results in a series of electrodes regularly disposed along the internal perimeter of the tube, as sketched in Figure 2.

As can be observed in this figure, the electrodes are in electrical contact with the fluid inside the tube, which is characteristic of conductance-based sensing strategies, in opposition with capacitance-based technique. Stainless steel was used in order to assure a higher electrical conduction in comparison to the fluid. Other important advantages of this material are its low cost, ease of fabrication and resistance to abrasion and corrosion. The distance between the rings (20 mm) as well as their width (20 mm) results from an optimization procedure, which minimized the error function (Favreau [20]). More specifically, the error function is defined as the ratio between the relative error in the determination of the thickness of a liquid film covering a pair of electrodes and the relative error in measuring the associated conductance (Coney [21]).

Several numerical and experimental simulations were performed in order to determine the qualitative behavior of the signals delivered by the probe with respect to the structure of the flow. As a general outcome, one can say that a current deficiency or excess (with respect to the values obtained when only the conducting phase is present in the probe) depends on the presence and on the shape of non-conducting inclusions within the sensing zone of each electrode. For instance, the presence of a non conducting structure (like a bubble) inside the sensing zone of a particular electrode results in a current deficiency at the relevant electrode and in a current excess at its neighbors. If the structure is larger (like an air plug), the current deficiency extends to several electrodes and the excess, although still present, is compensated by a total current reduction, which is a consequence of a global conductivity decrease. Therefore, the azimuthal current distribution at the measuring ring effectively varies considerably with the flow pattern and, more than that, reflects closely the geometry of the non-conducting phase flowing through the probe.

Another important feature, revealed by numerical simulations and confirmed by experiments, is the axial extent of the sensing volume. In the case of the pair of ring electrodes adopted here, this extent corresponds approximately to the distance between the rings taken from their centers, which is less than the extent associated to the usual electrode geometry employed in electrical tomographic imaging, defined by the measurement and the guard electrodes. A drawback of the geometry proposed in this work concerns a lower sensitivity at the core of the pipe when compared to the sensitivity

near the walls. Although this may be restrictive in some applications, the lost information is negligible at least with horizontal stratified flows, as will be demonstrated from the results presented in section 5.

4. EXPERIMENTAL FACILITY & TESTS

In order to illustrate the potentiality of the present direct imaging methodology, several experimental tests have been performed at the *Commissariat à l'Energie Atomique - Grenoble*, France. The measurements were carried out in a horizontal two-phase flow loop basically composed of an air circuit, a water circuit, a mixer, a test section and a separator. The test section, made in Plexiglas to allow flow visualization, is 30 m long and has an internal diameter of 60 mm. Special supports were designed in order to satisfy three basic requirements: dynamic neutrality (hydrodynamic forces do not generate mechanical vibrations), thermal stresses compensation and possibility to incline the test section. A laser beam and a set of targets placed along of the test section control its alignment and horizontality. The global misalignment does not exceed 3 mm over the total length. The loop's instrumentation includes temperature and pressure transducers and electromagnetic and turbine flow meters to measure respectively water and air flow rates. Two independent PID-based regulation loops control each of the flow rates, and allow to impose their temporal variations. It is important to stress that a careful choice of the PID parameters is fundamental for the loop's performance either in transient as well as in steady-state operation. This is related to the fact that the dynamic behavior of the two-phase loop depends on the flow pattern which can change abruptly and entirely during a transient test. A detailed description of the loop is provided by Selegim [22].

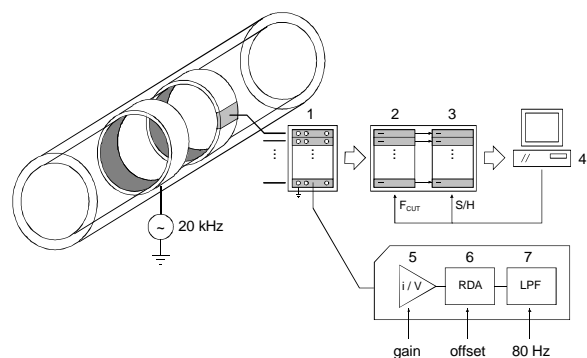


Figure 3: Measurement system.

The measurement system has 16 independent input channels and is basically composed of the current to voltage transducer modules, a signal conditioning chassis (National Instruments SCXI-1001) equipped with anti-aliasing filters (SCXI-1141) in series with sample

and hold circuits (SCXI-1140) and, an acquisition board (National Instruments AT-MIO-16E-5) installed on a microcomputer. This is depicted in Figure 3, which also reveals some details : current / voltage transducer (1), anti-aliasing filters (2), sample and hold circuits (3), microcomputer with acquisition board (4), current to voltage converter with gain control (5), rectifier with offset control (6) and forth-order low-pass Butterworth filter with $f_{cut} = 80$ Hz (7).

The experimental procedure consists essentially in doing transient tests in which the flow regime slowly evolves from one established configuration to another, crossing a transition in between. The test grid was set to exploit the maximum of the circuit's performance in the sense of reproducing all the main horizontal two-phase flow regimes. The trajectories in the flow map were generated by imposing either a constant gas flow rate or a constant water flow rate, allowing to cross the frontier between two different flow regimes as fast as possible. One flow rate being kept constant, the other is varied according to an imposed temporal law defined in three time intervals: a constant flow rate period, a ramp joining the starting and the ending flow rates and, another constant flow rate. The reason for the constant flow rate periods is to allow a good characterization of the starting and of the ending flow regimes. The test grid is defined in Table 1.

Flow regime	Q_{water} (m^3/h)	Q_{air} (m^3/h)	Duration (s)
Stratified	0.5	10 to 60	819.2
Slug to bubbly	5 to 50	7.5	819.2
Slug to annular	15	70 to 250	819.2

Table 1. Test grid.

5. RESULTS

In the following, results obtained from the tests described above will be presented. The signals delivered by the impedance probe (normalized current intensities) will be plotted as a function of time in abscissa and angular position θ of the associated electrode in ordinate, as defined in Figure 2. By this way, the horizontal lines near $\theta = 0$ and $\theta = 2\pi$ are representative of the bottom of the tube, and the lines near $\theta = \pm \pi$ correspond to the top of the tube. This juxtaposition of the time traces provides a flat or "unrolled" longitudinal view of the flow, as it is analogously done in Mercator's or other plane representation of the world globe. This is justified by the fact that the extent of the probe's sensing volume is negligible when compared to the length of the test section as well as to a characteristic length representative of the longitudinal evolution of the flow. The normalized current intensities are coded in gray levels ranging from white to black, which corresponds respectively to 0 and 100% of the

values obtained when the conducting phase fills the probe. In that way, water will appear in black and air in white in the following images.

5.1 Stratified flows

In stratified flow, gravity forces predominate over the other ones, producing a segregation between the liquid and the gas phases. The average liquid level and the geometry of the interface depend on the liquid and gas flow rates. Three stratified sub-regimes are commonly accepted. Classified by order of appearance when increasing the air flow rate and keeping the water flow rate constant, we can distinguish between: stratified smooth (flat interface); stratified wavy (the interface oscillates in a regular way) and stratified rugged (the interface oscillates randomly). In the case of horizontal configurations, the energy necessary to the formation of interface waves comes from the gas flow. Starting from a flat interface, the transition between stratified smooth and stratified wavy flows happens when the gas speed is high enough to destabilize the interface while maintaining the coherence of the waves, but not high enough to trigger the Kelvin-Helmholtz instability. Stable waves are characteristic of low gas flow rate values, while a rugged interface appears at higher gas flow rates. Although the physical mechanisms governing the generation of these waves are not completely known, it is generally accepted that pressure and shear forces must overcome the viscous dissipation in order to assure the existence of the waves, their coherent or random nature being probably correlated to the liquid height.

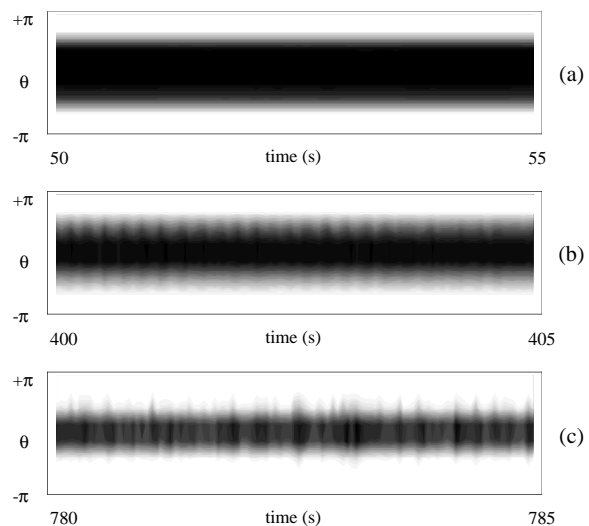


Figure 4: Imaged representation of stratified flows at constant $Q_{water} = 0.5$ m^3/h : a) smooth ($Q_{air} = 10$ m^3/h), b) wavy ($Q_{air} = 40$ m^3/h) and c) rugged ($Q_{air} = 60$ m^3/h). The sensing volume is flattened from the bottom.

Figure 4 illustrates the imaged representation of stratified smooth, wavy and rugged flows. In these pictures, the liquid height is indicated by the

thickness of the horizontal black zone in the center of the plots. The white strips at $\theta = \pm \pi$ reveal that the electrodes at the top of the pipe collect no signal because they are not wetted by the flow. As we can see, the flow patterns are easily recognizable by their main geometrical features. For these tests, the water flow rate was kept constant at $0.5 \text{ m}^3/\text{h}$ and the air flow rate values were respectively 10, 40 and $60 \text{ m}^3/\text{h}$. We can observe from the images that when the air flow rate increases, the liquid height decreases, which agrees with the stratified flow equilibrium equation (Taitel & Dukler [23]). Some finer details are also visible as, for instance, the distinct wave packets in stratified wavy flow and the presence of solitary large amplitude waves in stratified rugged flow (Seleghim [22]).

5.2 Intermittent to bubbly transition

Horizontal intermittent flow is characterized by a non-uniform liquid distribution in the axial direction. More precisely, liquid slugs fill the pipe and separate zones in which the gas flows on the top and the liquid flows on the bottom of the tube as in stratified flow. Consequently, the area void fraction is highly intermittent, alternating from a low value, associated to the presence of a liquid slug, to a higher one, associated to the stratified zone.

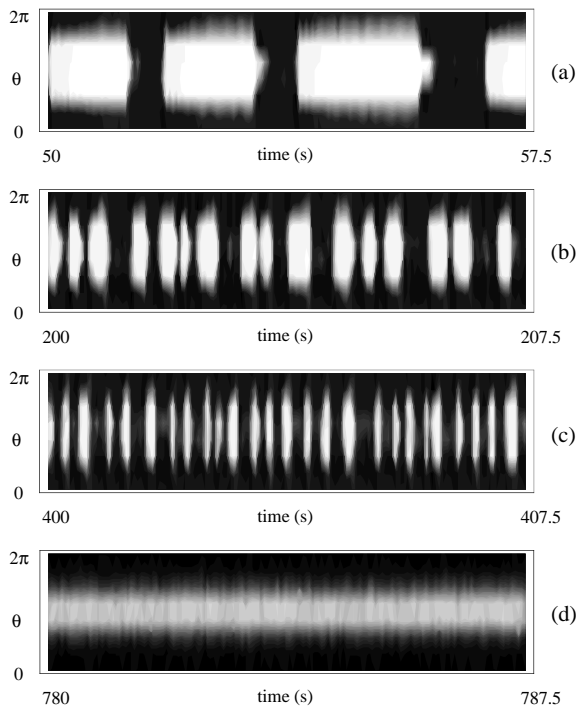


Figure 5: Imaged representation of intermittent and bubbly flows at constant $Q_{\text{air}} = 7.5 \text{ m}^3/\text{h}$: a) elongated bubbles ($Q_{\text{water}} = 5 \text{ m}^3/\text{h}$), b) medium aerated slugs ($Q_{\text{water}} = 15 \text{ m}^3/\text{h}$), c) small aerated slugs ($Q_{\text{water}} = 30 \text{ m}^3/\text{h}$) and d) bubbly flow ($Q_{\text{water}} = 50 \text{ m}^3/\text{h}$). The sensing volume is flattened from the top.

In Figure 5, θ ranges between 0 and 2π , which means that the signals collected by the electrodes at the top of the pipe are represented

at the center of the plots. We clearly see from Figure 5-a that these top electrodes are alternatively wet and dry, which respectively corresponds to liquid slugs and gas pockets passing through the sensor. Another feature revealed by Figures 5-a to 5-d is the absence of gas in the lowest part of the pipe, as indicated by the continuous black strips at $\theta = 0$ and $\theta = 2\pi$.

At low water flow rates, the liquid slug is not aerated and the corresponding area void fraction approaches zero. The stratified zones form what can be called elongated bubbles with a relatively sharp head and a biconvex rear end. Depending on the air flow rate, the surface of the liquid layer within the stratified zone may exhibit a wavy form, as we can observe on Figure 5-a.

When the water flow rate increases at constant air flow rate (thus towards bubbly flow), the forces that maintain the integrity of the air plugs, *i.e.* gravity and surface tension, start to compete with turbulent fluctuations which tend to entrain gas into the liquid slugs. This constitutes the basic mechanism for the transition between intermittent and bubbly flows. As a consequence of this gas entrainment, the water slugs become aerated with small bubbles increasing the local void fraction. The air plugs become smaller and faster, also due to the fact that, in intermittent flow, the increase of the water flow rate causes an increase on the global velocity of the two-phase structures (or group velocity) and therefore on the slugging frequency, which is a particularly important consequence in the scope of industrial applications. These features of the intermittent to bubbly transition can be observed in Figures 5-b and 5-c, while the established bubbly flow regime is shown in Figure 5-d. Due to the relatively low air flow rate, the bubbles are concentrated at the upper region of the tube which corresponds to the neighboring of $\theta = \pi$, but the gray strip at this location indicates that the top electrodes are always wetted by liquid.

5.3 Intermittent to annular transition

In the annular configuration, the liquid flows as a continuous film around the perimeter of the pipe, and is also continuous in the longitudinal direction, forming a liquid annulus. This liquid film surrounds a high-speed air flow at the core of the tube, which may contain entrained liquid droplets detached from wave crests at the liquid-gas interface. Under certain conditions near the transition to annular flow, circular aerated waves may be so that the film thickness increases substantially at the bottom as well as at the top of the tube. This is usually described as the wavy-annular flow pattern.

Starting from an intermittent flow, the annular regime is reached by increasing the air flow rate while keeping the water flow rate constant. The transition to annular flow takes place when the air flux is intense enough to break some of the water

slugs, generating liquid structures that are commonly identified as pseudo-slugs or rolling waves. An image of such a flow is proposed in Figure 6-a. The slugs that are not destroyed are highly accelerated, their velocity reaching that of the air flow. These very fast slugs wipe out the pipe and induce strong mechanical solicitations in the test section and in the separator because of their high kinetic energy. It is important to stress that in industrial applications, this operating condition may represent an important damage risk for the integrity of a multiphase facility, and is usually avoided.

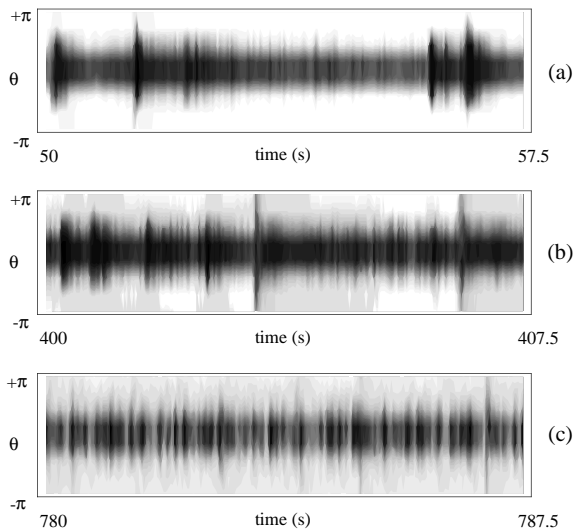


Figure 6: Imaged representation of the intermittent to annular transition (constant $Q_{\text{water}} = 15 \text{ m}^3/\text{h}$): a) pseudo-slugs or rolling waves ($Q_{\text{air}} = 70 \text{ m}^3/\text{h}$), b) fast slugs and drainage of the peripheral liquid film ($Q_{\text{air}} = 175 \text{ m}^3/\text{h}$) and c) established annular flow ($Q_{\text{air}} = 250 \text{ m}^3/\text{h}$). The sensing volume is flattened from the bottom.

Another important effect associated to the presence of fast slugs concerns the formation of the liquid film at the perimeter of the tube. If the gas velocity is not high enough to maintain this liquid film, it may flow back to the bottom of the tube, drying up the upper part of the test section, as can be observed in Figure 6-b. If the gas velocity is high enough to destroy all slugs and to maintain a stable liquid film flowing at the walls of the pipe, then the annular regime may be considered fully installed, as illustrated in Figure 6-c. The darkest horizontal strip at the center of the plot ($\theta = 0$) shows that, due to gravity, the liquid film is thicker at the bottom of the pipe, while the succeeding vertical strips reveal the occurrence of waves passing through the sensor.

6. CONCLUSION

A direct imaging probe suited for air-water flows is presented in this work. An imaged representation of the phase distribution within the probe's sensing volume is obtained by simply plotting the signals corresponding to peripheral conductivity measurements, therefore without any

numerical reconstruction from the measurements. To do so, the geometry of the probe's sensing electrodes has been optimized and consists basically of two stainless steel ring electrodes flush mounted inside the tube wall. The partition of the sensing volume, which is a fundamental requirement in direct imaging, is obtained by segmenting the measurement ring, what produces a series of electrodes regularly disposed according to the perimeter of the tube. Several experimental and numerical tests were performed aiming to determine the best excitation frequency, which minimizes contact impedance effects due to electrochemical phenomena taking place at the electrode interface, as well as to establish the qualitative behavior of the signals delivered by the probe with respect to the structure of the flow.

To demonstrate the potentiality of this imaging technique, a number of transient tests were conducted in a horizontal two-phase flow loop, which allows to impose temporal variations of the flow rates. The experimental procedure consists basically in slowly varying one flow rate while the other is kept constant, thus inducing a slow evolution of the flow regime from an established configuration to another, crossing a regime transition in between.

Results confirm that this direct imaging technique exhibits not only large structures such as slugs and plugs in intermittent flow for instance, but also finer details as the wavy or rugged liquid interface in stratified flow, or as the liquid film drainage occurring during the transition between intermittent and annular flows. It is obvious that the visual identification of the flow configuration as well as the regime transitions between them is quite straightforward. As a consequence, it has been demonstrated that this direct imaging methodology constitutes a simple and inexpensive alternative to tomographic imaging techniques, which are slowed down by the use of iterative numerical image reconstruction algorithm. In the particular field of industrial applications such as two-phase equipment monitoring, where qualitative and real time diagnostic is needed, the direct imaging technique offers an interesting technological answer. It is also important to stress that this imaging technique could be applied to non-conducting two-phase fluids, involving capacitive impedance measurements. This is of particular interest for gas-particulate flows such as in pneumatic transport pipelines, for fluidized bed combustion or even in the field of petroleum engineering.

Future developments of the imaging technique proposed here concern the influence of the measurement ring segmentation, *i.e.* how the final images can be improved or affected by a modification of the number and geometry of the electrodes. In particular this could lead to sensor

configurations providing more information concerning the flow structure in the core of the pipe.

ACKNOWLEDGMENTS

This work was performed at the CEA-Grenoble under the auspices of the Service de Thermohydraulique pour les Applications Industrielles, at the Laboratoire d'Etudes Fondamentales. Additional funding was provided by the Brazilian Research Council - CNPq through the Ph.D. studentship to PSJr. (proc. 201684/91-8).

REFERENCES

- [1] Lemonnier H. & Peytraud J.F., "Is 2D impedance tomography a reliable technique for two-phase flows?", Proc. OECD/CSNI Specialist meeting on advanced instrumentation and measurement techniques, Santa Barbara, CA, March 17-20, 1997.
- [2] Seo J.K., "On the uniqueness of the inverse conductivity problem", J. of Fourier Analysis and Applications, 1996, **2**, N°2-4.
- [3] Herman G.T., "Image Reconstruction from Projections - The Fundamentals of Computerised Tomography", Academic Press, New York, 1980.
- [4] Natterer F., "The Mathematics of Computerised Tomography", Wiley, Chichester, 1986.
- [5] Caorsi S., Gagnani G.L. & Pastorino M., "A multiview microwave imaging system for two-dimensional penetrable objects", IEEE Trans. Microwave Theory, 1991, **39**, pp.845-851.
- [6] Chiu C. & Kiang Y.W., "Electro-magnetic imaging for imperfectly conducting cylinder", IEEE Trans. Microwave Theory, 1991, **39**, pp.1632-1639.
- [7] Huang S.M., Xie C.G., Thorn R., Snowden D. & Beck M.S., "Design of sensor electronics for electrical capacitance tomography", IEE Proc. , 1992, **G-139**, pp.83-88.
- [8] Xie C., Huang S.M., Hoyle B.S., Thorn R., Lenn C., Snowden D. & Beck M.S., "Electrical capacitance tomography for flow imaging: system model for development of image reconstruction algorithms and primary sensors", IEE Proc. , 1992, **G-139**, pp.89-98.
- [9] Isaksen Ø. and Nordtvedt J.E., "A new reconstruction algorithm for use with capacitance-based process tomography", Modeling Identification Control, 1992, **19**, pp.9-21.
- [10] Kim Y. and Woo H.W., "A prototype system and reconstruction algorithms for electrical impedance technique in medical body imaging", Clin. Physiol. Measurements, 1987, **A-8**, pp.63-70.
- [11] Yorkey T.J., Webster J.G. & Tompkins W.J., "An improved perturbation technique for electrical impedance imaging with some criticisms", IEEE Trans. Biomed. Eng. , 1987, **34**, pp.898-901.
- [12] Yorkey T.J., Webster J.G. & Tompkins W.J., "An optimal impedance tomographic reconstruction algorithm", Proc. An. Int. Conf. IEEE Eng. Med. Biol. Soc., 1986, **8**, pp.339-342.
- [13] Abdullah M.Z., Quick S.V. & Dickin F.J., "Quantitative algorithm and computer architecture for real-time image reconstruction in process tomography", Proc. of the 1st Meeting on European Concerted Action on Process Tomography, 1992, 26-29 March, Manchester, pp.179-192, Ed. M.S. Beck.
- [14] Williams R.A. & Beck M.S., "Introduction to process tomography. Process Tomography", Williams & Beck Eds., Butterworth-Heinemann, 1995.
- [15] Gisser D.G., Isaacson D. & Newell J., "Current topics in impedance imaging", Clin. Phys. Physiol. Meas., 1987, **A-8**, pp.36-46.
- [16] Peytraud J.F., "Etude de la tomographie électrique pour la mesure du taux de vide local en écoulements diphasiques", Thèse de doctorat, INP Grenoble, Spéc. Energétique Physique, 1995.
- [17] Klug F. & Mayinger F., "Impedance based flow reconstruction - a novel flow composition measuring technique for multiphase flows", Nucl. Eng. and Design, 1994, **146**, pp.35-42.
- [18] Asali J.C., Hanratty T.J. & Andreussi P., "Interfacial drag and film height for vertical annular flow", AIChE J. , 1985, **31**, pp.895-902.
- [19] Andreussi P., Di Donfrancesco A. & Messia M., "An impedance method for the measurement of liquid hold-up in two-phase flow", Int. J. Multiphase Flow, 1988, **14**, N°6, pp.777-785.
- [20] Favreau C., Internal Report – Commissariat à l'Energie Atomique - Grenoble, 1993.
- [21] Coney M.W.E., "The theory and application of conductance probes for the measurement of liquid film thickness in two-phase flow", J. Physics E: Scientific Instruments, 1973, **6**, pp. 903-910.
- [22] Seleglim Jr. P., "Caractérisation des changements de configuration d'un écoulement diphasique horizontal par l'application de méthodes d'analyse temps-fréquence", Thèse de doctorat, INP Grenoble, Spéc. Mécanique, 1996.
- [23] Taitel Y. & Dukler A.E., "A model for predicting flow regime transitions in horizontal and near horizontal gas-liquid flow", AIChE Journal, 1976, **22**, N°1, pp. 47-55.